Article

Evaluating the Performance of Sentinel-2, Landsat 8 and Pléiades-1 in Mapping Mangrove Extent and Species

Dezhi Wang [1,2] **, Bo Wan** [1,2] **, Penghua Qiu** [3,*] **, Yanjun Su** [4] **, Qinghua Guo** [4,5] **, Run Wang** [1,2] **, Fei Sun** [1,2] **and Xincai Wu** [1,2]

[1] Faculty of Information Engineering, China University of Geosciences (Wuhan), Wuhan 430074, China; wuhan1990hk@126.com (D.W.); magicwan1105@163.com (B.W.); runwang@cug.edu.cn (R.W.); sf_rs2007@cug.edu.cn (F.S.); wuxincai@mapgis.com (X.W.)
[2] National Engineering Research Center of Geographic Information System, Wuhan 430074, China
[3] College of Geography and Environmental Science, Hainan Normal University, Haikou 571158, China
[4] State Key Laboratory of Vegetation and Environmental Change, Institute of Botany, Chinese Academy of Sciences, Beijing 100093, China; suyanjun1987@gmail.com (Y.S.); guo.qinghua@gmail.com (Q.G.)
[5] University of Chinese Academy of Sciences, Beijing 100049, China
[*] Correspondence author: cphscnu@163.com; Tel.: +86-0898-6588-4244

Abstract: Mapping mangrove extent and species is important for understanding their response to environmental changes and for observing their integrity for providing goods and services. However, accurately mapping mangrove extent and species are ongoing challenges in remote sensing. The newly-launched and freely-available Sentinel-2 (S2) sensor offers a new opportunity for these challenges. This study presents the first study dedicated to the examination of the potential of original bands, spectral indices, and texture information of S2 in mapping mangrove extent and species in the first National Nature Reserve for mangroves in Dongzhaigang, China. To map mangrove extent and species, a three-level hierarchical structure based on the spatial structure of a mangrove ecosystem and geographic object-based image analysis is utilized and modified. During the experiments, to conquer the challenge of optimizing high-dimension and correlated feature space, the recursive feature elimination (RFE) algorithm is introduced. Finally, the selected features from RFE are employed in mangrove species discriminations, based on a random forest algorithm. The results are compared with those of Landsat 8 (L8) and Pléiades-1 (P1) data and show that S2 and L8 could accurately extract mangrove extent, but P1 obviously overestimated it. Regarding mangrove species community levels, the overall classification accuracy of S2 is 70.95%, which is lower than P1 imagery (78.57%) and slightly higher than L8 data (68.57%). Meanwhile, the former difference is statistically significant, and the latter is not. The dominant species is extracted basically in S2 and P1 imagery, but for the occasionally distributed *K. candel* and the pioneer and fringe mangrove *A. marina*, S2 performs poorly. Concerning L8, S2, and P1, there are eight (8/126), nine (9/218), and eight (8/73) features, respectively, that are the most important for mangrove species discriminations. The most important feature overall is the red-edge bands, followed by shortwave infrared, near infrared, blue, and other visible bands in turn. This study demonstrates that the S2 sensor can accurately map mangrove extent and basically discriminate mangrove species communities, but for the latter, one should be cautious due to the complexity of mangrove species.

Keywords: mangroves; species; Sentinel-2; Landsat 8; Pléiades-1; random forest

1. Introduction

Mangroves are salt-tolerant evergreen woody plants and grow in the inter-tidal region in the tropics and subtropics, distributed in 118 countries and regions, with a total global area of about 137,760 km^2 [1]. They play an important role in windbreaks, shoreline stabilization and maintenance of ecological balance and biodiversity [2]. Though mangroves provide a wide range of ecosystem services and goods, global mangrove forests declined by 35% from 1980 to 2000 due to conversion to agricultural land, aquaculture ponds, and construction land [2,3]. Mangrove forests in China have also been largely damaged, decreasing from 420 km^2 in the 1950s to 220 km^2 by 2000 [4]. It is crucial, therefore, to monitor the extent and species of mangrove forests against land use change and forest ecosystem degradation.

Remote sensing provides an accurate, efficient, and repetitive method of mapping and evaluating mangroves. Due to the special growth environment of mangroves (inter-tidal mudflats inundated by periodic seawater) and their dense forests, it is very difficult for people to enter mangrove forests for extensive field surveying and sampling. Therefore, remote sensing data have been widely used for evaluating mangroves in the past two decades [5,6], such as for mapping the distribution of global mangroves [1], monitoring the extent and dynamics of national [7–9] or regional [10–12] mangroves, identifying species composition of local mangroves [13–15], and estimating biophysical indicators [16,17].

Regarding mapping mangrove extent, medium-resolution multispectral imagery is the most popular data. Chen et al. (2017) [18] employed a larger number of 30-m Landsat 7/8 images combined with Sentinel-1A imagery to map China's mangroves. Leon et al. (2017) [19] used multi-temporal 10-m SPOT imagery to uncover the spatial-temporal dynamics of land cover change and fragmentation of mangroves. However, the spatial and spectral information provided by these medium-resolution multispectral data might not be enough for studying mangrove forests and their species composition in detail. Narrow extent mangroves (<30 m) or isolated mangrove assemblages (<900 m^2) always exist along coastlines, for example. To discriminate the types of mangrove species, the most popularly used data are commercial high-resolution multispectral imagery, followed by hyperspectral imagery. Wang et al. (2004) [20], for example, compared the performances of IKONOS and QuickBird data in classifying mangrove species on the Caribbean coast of Panama. Heenkenda et al. (2014) [13] and Zhu et al. (2017) [17] all used WorldView-2 to demarcate mangrove species. Few researchers have used medium-resolution imagery for mangrove species classification. Pham and Brabyn (2017) [21] utilized 10-m SPOT 4/5 images to identify three mangrove associations, for example. While the use of high-resolution imagery has gained considerable attention, their limitations of high purchase cost and small swath size hampers continuous or large geographic coverage monitoring. Therefore, the mapping of large-scale mangrove forest extent and species composition might lie in the ability of emerging sensors.

Sentinel-2A, the first of the two identical satellites, was launched on 23 June 2015; Sentinel-2B, the second, was launched on 7 March 2017. Sentinel-2 offers 13 multispectral bands, of which four traditional bands (red/green/blue/near infrared) have a spatial resolution of 10-m and three bands are red-edge bands designed for vegetation detection [22]. Sentinel-2 data has been used for vegetation [23], such as estimating boreal forest canopy cover and the leaf area index [24], mapping C3 and C4 grass species [25], and predicting forest growing stock volumes [26,27], but they are rarely used for mangroves. Due to the limitations of WorldView-2 (such as data complexity, high cost, and small swath size) and Landsat 8 imagery (such as lack of red-edge band, medium spatial, and temporal resolution), Shapiro et al. (2015) [28] and Pastor et al. (2015) [29] have suggested using Sentinel-2 imagery for mangrove extent monitoring and mangrove chlorophyll concentration estimation, respectively. Castillo et al. (2017) [16] evaluated the ability of Sentinel-1 and Sentinel-2 for the retrieval of above group biomass of mangroves and their replacement land uses. Their results showed that red-edge bands performed better than visible and short wave infrared bands. Valderrama et al. (2018) [30] compared Landsat 8, SPOT-5, Sentinel-2, and WorldView-2 in classifying three mangrove species

groups, but they only used threshold values of normalized difference vegetation index (NDVI) to distinguish species. Therefore, it is necessary to explore whether the newly-launched Sentinel-2 can bring new opportunities for the classifications of mangrove extent and species.

Landsat 8, launched on 11 February 2013, has 11 bands, of which the spatial resolution of the panchromatic band is 15-m. Compared with previous Landsat satellites, the lengths of the red, near-infrared, and shortwave infrared bands were narrowed, radiation resolution was increased to 16 bits, and signal-to-noise ratio was significantly improved. These advances improved the ability of Landsat 8 for vegetation discriminations. Landsat 8 data have been used for extracting mangrove spatial coverage [9,31,32], canopy cover [33], and carbon stock [34,35], but they are rarely utilized in mangrove species community classifications. The Pléiades-1 (Pléiades-1B, launched on 1 December 2012) is a very high spatial resolution sensor, which has been used by Wang et al. (2018) [15] in the classification of artificial mangrove species. Hence, Pléiades-1 and Landsat 8 were selected as comparison data for Sentinel-2.

When comparing the potential of remote sensing data in mapping and evaluating mangroves, most studies focused on a specific scale such as mangrove extent, zonation or species. However, mangrove extent and species are both important for mangrove protection and management, and they have attracted a lot of interest during the past two decades [5,36]. Therefore we evaluated the performance of Sentinel-2 at mangrove extent scale and mangrove species community scale. Studying at different spatial scales and temporal frequencies, where the related mangrove landscape patterns and processes occur, can help researchers understand mangrove responses to environmental changes.

Against this background, the present study aims to examine the potential of newly-launched Sentinel-2 in extracting two-scale mangrove features, namely mangrove extent and mangrove species community, and evaluate the importance of spectral bands and object features in a typical mangrove reserve in Hainan, China. The performance is also examined against that of Landsat 8 and Pléiades-1. The following four questions will be addressed: (1) How to use Landsat 8, Sentinel-2, and Pléiades-1 data to classify mangrove extent and species communities? (2) How are the classification accuracies and the performance of the three sensors at the two scales? (3) Which object features (such as red-edge bands, vegetation indices or texture information) are more important for the discrimination of mangrove species? (4) Can the free and global Sentinel-2 sensor open a new window for mangrove species classifications? Solving these problems will not only help to obtain the mangrove extent and species quickly and accurately, but will also provide a reference for geophysicists, ecologists, and mangrove managers to select remote sensing images.

2. Data and Methods

2.1. Study Area

The study area is located in the northeastern area of Hainan island, including Dongzhaigang National Nature Reserve (DNNR) and its surrounding area, about 2 km outside (Figure 1). DNNR is the first National Nature Reserve for mangroves in China and a Wetland of International Importance under the Ramsar Convention. It is a typical mangrove wetland in China, consisting of the major mangrove species in southern China. It covers a total area of 3337.6 ha, of which about 1578 ha is mangrove forests. The site is characterized by a tropical monsoon climate with an annual average temperature of 23.8 °C, an annual precipitation of 1615 mm and a rainy season between May and September. The mangrove species in DNNR is very rich, and *Bruguiera sexangula*, *Bruguiera gymnorrhiza*, *Ceriops tagal*, and *Rhizophora stylosa* are dominant species.
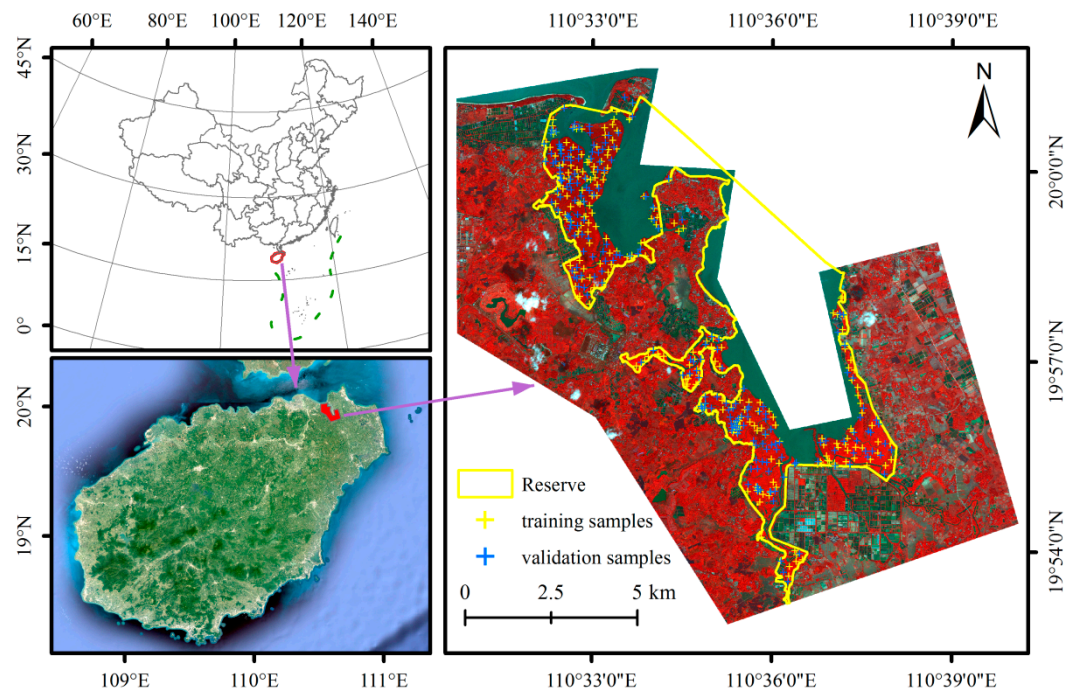
Figure 1. The location and false color combination of 0.5-m Pléiades-1 data (Near infrared, Green, and Blue bands) of the study area.

2.2. Remote Sensing Data and Pre-Processing

The characteristics of the Sentinel-2A MSI (S2), Landsat 8 OLI (L8) and Pléiades-1B (P1) images are presented in Table 1. The P1 imagery was acquired on 4 February 2014. The S2 and L8 imagery was acquired on 9 December and 14 February 2016, respectively, due to a cloud-free, dry season similar to the acquisition data of the Pléiades-1 imagery.

The S2 satellite images (Level-1C) were downloaded from the European Space Agency's (ESA) Sentinel Scientific Data Hub (https://scihub.copernicus.eu/dhus/#/home), which were orthorectified and top-of-atmosphere images. Using the sen2cor atmospheric correlated processor (version 2.4.0), which is an inbuilt algorithm within the software SNAP (Sentinel's Application Platform) version v6.0, the authors processed the acquired Level-1C images and got bottom-of-atmosphere Level-2A products. The L8 images were downloaded from the United States Geological Survey (USGS, https://earthexplorer.usgs.gov/), and the Pléiades-1 images were purchased from the supplier (DigitalGlobal, Longmont, CO, USA). Atmospheric correction was also performed for the L8 and P1 imagery. First, digital numbers of images were converted to at-sensor radiance values. Second, the radiance values were converted to bottom surface reflectance using the FLAASH (Fast Line-of-Sight Atmospheric Analysis of the Spectral Hypercube) model in ENVI 5.3 (Harris Geospatial, Melbourne, FL, USA). The atmospheric correction of L8 and P1 imagery did not take real-time water vapor profile into consideration due to the lack of 820/940/1135 nm bands. However, according to Song et al. (2001) [37], as soon as a comparison between different sensors is carried out with imagery expressed in the same relative scale, the influence of atmosphere on the classification results can be neglected [26]. The cirrus band (B9 in L8, B10 in S2) was excluded from the analysis as it was dedicated to detecting cloud.

Table 1. The characteristics of Landsat 8, Sentinel-2 and Pléiades-1 imagery.

Spectrum	Landsat 8 2016-2-14				Sentinel-2A 2016-12-9				Pléiades-1B 2014-2-4			
	Band	Centre (nm)	Wave Width (nm)	Spatial Resolution (m)	Band	Centre (nm)	Wave Width (nm)	Spatial Resolution (m)	Band	Centre (nm)	Wave Width (nm)	Spatial Resolution (m)
Aerosol	B1	443	16	30	B1	442.3	45	60				
Blue	B2	482.6	60.1	30	B2	492.1	98	10	B1	495	76.5	2
Green	B3	561.3	57.4	30	B3	559	46	10	B2	558.5	83.7	2
Pan	B8	591.7	172.4	15	-	-	-	-	B5	652.5	326.8	0.5
Red	B4	654.6	37.5	30	B4	665	39	10	B3	656	78.8	2
Red edge-1	-	-	-	-	B5	703.8	20	20	-	-	-	-
Red edge-2	-	-	-	-	B6	739.1	18	20	-	-	-	-
Red edge-3	-	-	-	-	B7	779.7	28	20	-	-	-	-
NIR	-	-	-	-	B8	833	133	10	-	-	-	-
NIR	B5	864.6	28.2	30	B8a	864	32	20	B4	842.5	130.3	2
Water vapor	-	-	-	-	B9	943.2	27	60	-	-	-	-
Cirrus	B9	1373	20.4	30	B10	1376.9	76	60	-	-	-	-
SWIR-1	B6	1609	84.7	30	B11	1610.4	141	20	-	-	-	-
SWIR-2	B7	2201	186.7	30	B12	2185.7	238	20	-	-	-	-

Regarding S2, all bands were resampled to 10-m spatial resolution using nearest neighbor method and constituted an image stack. Concerning P1 and L8, in order to utilize both the high spatial and spectral resolution options for mangrove species classification [13], the multispectral imagery was pan-sharpened by the panchromatic imagery to produce 0.5-m and 15-m imagery, respectively, using the NNDiffuse spectral sharpening tool in ENVI 5.3 [38]. Finally, the L8 and S2 images were geo-referenced based on the 0.5-m P1 image with the accuracy of less than 0.5 pixel.

2.3. Field Survey

An extensive field survey was conducted in DNNR from February to June 2014, with the help of the DNNR authority. The purpose of this survey is to investigate the mangrove species distributions at a community level using a Real-Time Kinematic (RTK) Global Navigation Satellite System (GNSS) with centimeter level spatial accuracy based on continuously operating reference stations (CORS). The shape of the sample is circular or approximately square. The sample points were randomly generated first but, to ensure every target species held enough samples, some point locations were modified. A few hard-to-access points were visually interpreted by 0.5-m P1 and Google Earth imagery, while consulting the staff at the reserve simultaneously or moved to other places. Finally, the authors collected a total of 450 field samples (Figure 1). During April to May 2017, the authors conducted another field survey to investigate the changes to the area, as compared to the results from 2014. The reason why we conduct another field survey is that a few of fringe mangroves were damaged in July 2014 by a typhoon. Several field samples were moved to the same mangrove communities nearby according to the second field survey. This modification was to make sure all the samples not only keep representative, but also keep stable in the past two years.

Through surveys, there were mainly 17 kinds of mangrove species found in the DNNR, of which *Bruguiera sexangula*, *Bruguiera gymnoihiza*, *Ceriops tagal*, and *Rhizophora stylosa* were dominant species accounting for nearly 80% of the total area [39]. Based on mangrove species characteristics and community structures, the 17 species were divided into six species communities: *Bruguiera sexangula* (*B. sexangula*), *Ceriops tagal* (*C. tagal*), *Rhizophora stylosa* (*R. stylosa*), *Kandelia candel* (*K. candel*), *Avicennia marina* (*A. marina*) and *Lumnitzera racemosa* (*L. racemos*). *Bruguiera gymnoihiza*, and *B. sexangula* belonged to the same genus of Rhizophora, and showed high similarly and tended to be distributed together in some of the study areas, thus they were merged as the *B. sexangula* community. All samples were divided into two sets at field-level, based on their spatial distribution, with one set designed for training and the other for assessing classification accuracy (Table 2).

Table 2. Number of training and validating samples for each mangrove species.

Species	Training Samples (Average Area about 1000 m², Min Area ≥300 m²)	Validation Samples (Center Point)
Bruguiera sexangula	55	48
Ceriops tagal	55	48
Rhizophora stylosa	55	48
Kandelia candel	25	22
Avicennia marina	25	22
Lumnitzera racemosa	25	22
Sum	240	210

2.4. Two-Scale Mangrove Features Classifications

The mangrove composition of the study area was divided into three levels, namely landscape, vegetation cover type, and tree species community. Figure 2 shows the hierarchical structure of mangrove features and presents the objects of interest to be mapped. Found in the hierarchy, every "super-level" object acts as a container for its "sub-level" objects, and works with a parent and child relationship, while objects at the same level have a neighborhood relationship [40]. The object-based image analysis approach

was used to implement the hierarchy. Creating an object-based classification mainly consists of two steps: Image segmentation and object classification. Table 3 shows the rule sets and classification processes developed for the Dongzhaigang wetland, in which some spectral indices are selected and combined and some new spectral indices are proposed.
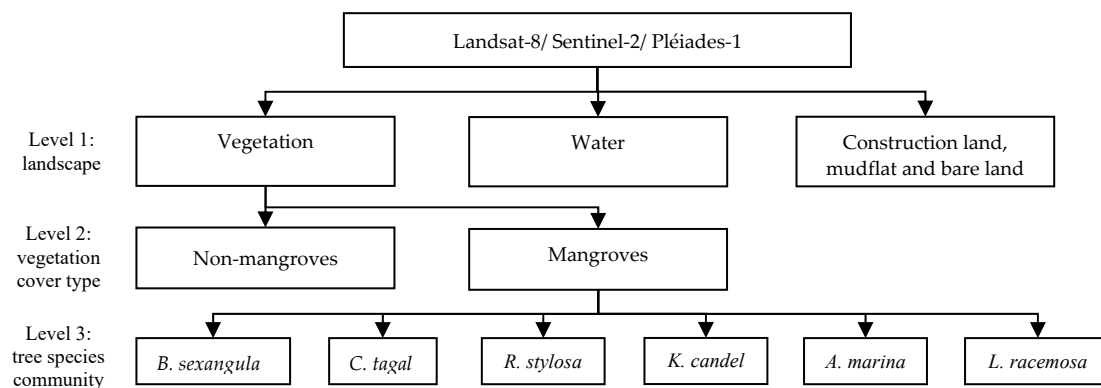

Figure 2. Image object hierarchy for two-scale mangrove feature classifications.

Table 3. Two-scale mangrove feature classifications based on Landsat 8, Sentinel-2 and Pléiades-1. MNDWI represents modified normalized difference water index; FDI represents forest discrimination index; WFI represents wetland forest index; MDI2 represents mangrove discrimination index 2; NDWI represents normalized difference water index; NDVI represents normalized difference vegetation index; Red represents the red band; NIR represents the near infrared band; and Seg is an abbreviation for segmentation.

Level		Landsat 8 15 m	Sentinel-2 10 m	Pléiades-1 0.5 m
Level 1	water	Chessboard Seg: 1 MNDWI > 0 FDI < 0	Chessboard Seg: 1 MNDWI > 0 FDI < 0 Brightness < 1250	Multiresolution Seg: 500 NDWI ≥ −0.25 Brightness < 2000
	vegetation	WFI > 1.2	WFI > 0.7	NDVI > 0.4
	Construction land, mudflat and bare land	Not "Vegetation" or "Water"	Not "Vegetation" or "Water"	Not "Vegetation" or "Water"
Level 2	Mangrove	Multiresolution Seg: 80 MDI2 > 3.4	Multiresolution Seg: 64 MDI2 > 4.7	Multiresolution Seg: 500 300 < Red < 660 4200 < NIR < 6000
	Non-mangrove	Not "Mangroves"	Not "Mangroves"	Not "Mangroves"
Level 3	Mangrove species community	Multiresolution Seg: 30 Random Forest in R	Multiresolution Seg: 30 Random Forest in R	Multiresolution Seg: 350 Random Forest in R

The first level was used to discriminate vegetation and non-vegetation and produced a mask of vegetation. A chessboard segmentation with an object size of one pixel was applied to L8 and S2 images in eCognition Developer 9.0 (Trimble, Sunnyvale, CO, USA), respectively, which preserved the pixel value of coarse or moderate resolution images. Thus, the fringe and isolated vegetation including mangroves could be preserved at the first step and for further classification. Using P1, due to its very high resolution, the chessboard segmentation was replaced by the multi-resolution segmentation (MRS) [41]. The MRS, with a scale of 500, was used to divide the image into spectrally homogeneous objects or pixel groups, which could decrease the internal spectral discrepancy (intra-class variability) of each landscape class and increase the spectral discrepancy between different classes (inter-class variability) for very high spatial resolution imagery [15]. The scale of 500 for P1 was chosen from the iterative "trail and error" approach [42]. The specific description of MRS can be found in Reference [41] and an application to remote sensing can be found in Reference [42]. Following segmentation,

the objects with the Modified Normalized Difference Water Index (MNDWI, Equation (1)) [43] higher than zero and the Forest Discrimination Index (FDI, Equation (2)) [40] less than zero were classified as water in S2 (Table 3). Only using MNDWI caused some fringe mangroves like *A. marina* to present as water. Since the FDI of vegetation was greater than zero, the combination of FDI and MNDWI could exclude fringe mangroves and precisely extract water. Moreover, due to some of mudflat overlapping with water and the brightness of the mudflat being greater than water, the brightness was used as supplement to exclude these mudflats. To identify vegetation, based on the surface feature spectrum (Figure A2), the authors proposed a new index—the Wetland Forest Index (WFI, Equation (3))—to extract vegetation, which was more accurate than NDVI (Normalized Difference Vegetation Index) [15] and FDI in the study area. For example, based on S2 imagery, the producer's accuracy (Pa) and the user's accuracy (Ua) of vegetation using WFI was 97.07% and 86.17%, respectively, through 968 validation samples of each images, which are randomly produced in ArcGIS (ESRI, Redlands, CA, USA) and visually interpreted for level 1. While, the Pa and Ua of NDVI greater than 0.4 are 93.66% and 82.74%, followed by FDI greater than 200 (Pa = 93.43%, Ua = 82.40%). The objects with WFI greater than 0.7 were classified as vegetation. The remaining objects at level one were classified as "construction land, mudflat and bare land". Subsequent to level one classification, the authors generated a mask of vegetation. For L8 data, the authors utilized MNDWI and FDI to identify water, and used WFI greater than 1.2 to extract vegetation. Regarding Pléiades-1, water was recognized using NDWI [15] and Brightness [15], and vegetation was mapped utilizing NDVI greater than 0.4. Through accuracy assessment using the above mentioned 968 validation samples, all the images could correctly extract vegetation with overall classification accuracies higher than 93%.

$$\text{MNDWI} = (\text{Green} - \text{SWIR-1})/(\text{Green} + \text{SWIR-1}) \tag{1}$$

$$\text{FDI} = \text{NIR} - (\text{Red} + \text{Green}) \tag{2}$$

$$\text{WFI} = (\text{NIR} - \text{Red})/\text{SWIR-2} \tag{3}$$

The second level was used to separate mangrove from non-mangrove within the vegetation mask produced in level 1. MRS with scale parameters of 80, 64, and 500 were applied to L8, S2, and P1, respectively. The scale parameters of L8 and S2 were obtained from the ESP (Estimation of Scale Parameters) [44] method, and P1 was obtained through the iterative "trail and error" approach [42], due to its large data and being time consuming. Since mangroves had a lower spectral reflectance in the shortwave infrared bands (SWIR) than terrestrial vegetation did (Figure A2), the authors created a new Mangrove Discrimination Index 2 (MDI2, Equation (4)) for separating mangroves from other vegetation, which could magnify the discrepancy of SWIR-2 between mangroves and non-mangroves. The authors have compared the performance of SWIR-1, SWIR-2, NIR, red edge bands, and MDI1 (similar to MDI2, but replace SWIR2 with SWIR1) with MDI2 in separating mangroves from non-mangroves in eCongnition Developer 9.0 by the visual examination method. The results showed that MDI2 performed best in S2 and L8 imagery. Employing Sentinel-2, mangroves were identified by an MDI2 higher than 4.7. Applying Landsat 8, the objects with MDI2 higher than 3.4 were classified as mangroves. Since NIR and red bands were found useful in demarcating mangroves in high resolution images [15,40], for Pléiades-1, the authors employed NIR and red bands to extract mangroves after analyzing mangrove and non-mangrove vegetation spectrum (Figure A2).

$$\text{MDI2} = (\text{NIR} - \text{SWIR-2})/\text{SWIR-2} \tag{4}$$

The third level was designed to discriminate mangrove species communities. The segmentation scale was set to 30, 30, and 350 for L8, S2 and P1 through the iterative "trail and error" approach, respectively. Following the selection of spectral and textural features, these mangrove objects were classified in R 3.5.0 (a multi-platform, open-source language and software for statistical computing) using varSelRF and random Forest packages.

2.5. Spectral and Textural Features

Regarding mangrove species classifications at level 3, three kinds of object features were selected: original spectral bands, spectral indices, and texture features (Table 4). These features were selected based on their previous performances in mangrove species discriminations, mangrove biomass inversions or other vegetation studies, as highlighted in literature [14,24,25,45–48]. EVI (enhanced vegetation index), for example, enhances vegetation signals by adding blue bands to correct soil background and aerosol scattering effects, which is suitable for areas with high leaf area index values [17]. The spectral features consisted of conventional NIR indices, red edge indices and shortwave infrared indices. Texture features comprised homogeneity, contrast, entropy, and correlation, which were calculated from individual image bands through a gray level co-occurrence matrix (GLCM) with a distance of one in four directions (0°, 45°, 90°, and 135°) [49]. Finally, there were 126, 218, and 73 features for L8, S2, and P1 in mangrove species classification, respectively.

2.6. Random Forest Classification, Feature Selection and Parameters Tuning

Random forest (RF) classification is an ensemble machine learning algorithm for supervised classification through the use of combined multiple decision trees, which obtains final results by averaging the class assignment probabilities from all produced trees [50,51]. The trees are created by drawing a subset of training samples through replacement (a bagging approach, also known as bootstrap aggregation) and randomly selecting variables. Compared with other machine learning algorithms, the RF algorithm has advantages in classifying high-dimensional and confusing objects, and can estimate the importance of predictor variables [50,52]. Therefore, the authors selected RF algorithm in the current study.

During each bootstrap training set, approximately two/three of the samples (in-bag samples) from the original dataset are used to train the trees, while the remaining dataset (out-of-bag samples) are used in an internal cross-validation for assessing how the resultant RF model performs [50,51]. The error estimate using the out-of-bag (OOB) samples is known as the OOB error. The OOB data are also used to measure the importance of predictor variables like in the following steps:

1) Given the input predictor variables of size m, randomly permute the values of the ith (i = 1, 2, ... , m) variable in the OOB samples;
2) Run the changed OOB data in the corresponding tree and obtain the *errOOB 2* (OOB error 2), and the OOB error of the original data in the tree is named *errOOB 1*;
3) Repeat step (1) and (2) for all trees (*ntree*), and calculate the mean decrease accuracy (MDA) [53] for variable i by $\sum(errOOB\ 2 - errOOB\ 1)/ntree$;
4) Repeat step (1), (2), and (3) for each predictor variable and obtain its mean decrease accuracy.

Table 4. A list of object features for mangrove species classifications.

Object Features		Formula for Landsat 8	Formula for Sentinel-2	Formula for Pléiades-1	Reference
Spectral Bands	Individual Bands	B1, B2, B3, B4, B5, B6, B7	B1, B2, B3, B4, B5, B6, B7, B8, B8a, B9, B11, B12	B1, B2, B3, B4	*NA*
Conventional NIR indices	DVI	*B5 − B4*	*B8 − B4*	*B4 − B3*	[45]
	CIg	*(B5/B3) − 1*	*(B8/B3) − 1*	*(B4/B2) − 1*	[48]
	SR	*B5/B4*	*B8/B4*	*B4/B3*	[45]
	NDVI	*(B5 − B4)/(B5 + B4)*	*(B8 − B4)/(B8 + B4)*	*(B4 − B3)/(B4 + B3)*	[46]
	EVI	$\frac{2.5\times(B5-B4)}{B5+6\times B4-7.5\times B2+1}$	$\frac{2.5\times(B8-B4)}{B8+6\times B4-7.5\times B2+1}$	$\frac{2.5\times(B4-B3)}{B4+6\times B3-7.5\times B1+1}$	[24]
Red edge indices	CIre1	*NA*	*B5/B3-1*	*NA*	[47]
	CIre2	*NA*	*B6/B3-1*	*NA*	[47]
	CIre3	*NA*	*B7/B3-1*	*NA*	[47]
	NDVIre1	*NA*	*(B8 − B5)/(B8 + B5)*	*NA*	[25]
	NDVIre2	*NA*	*(B8 − B6)/(B8 + B6)*	*NA*	[25]
	NDVIre3	*NA*	*(B8 − B7)/(B8 + B7)*	*NA*	[25]
	MSR$_{ren}$	*NA*	$\frac{(B8a/B5)-1}{\sqrt{(B8a/B5)+1}}$	*NA*	[47]
Shortwave infrared indices	MDI1	*(B5 − B6)/B6*	*(B8 − B11)/B11*	*NA*	*NA*
	MDI2	*(B5 − B7)/B7*	*(B8 − B12)/B12*	*NA*	*NA*
Texture information	Homogeneity	$\sum_{i,j=1}^{N_g}\frac{GLCM(i,j)}{1+\lvert i-j\rvert}$	*the same to left*	*the same to left*	[14]
	Contrast	$\sum_{i,j=1}^{N_g}(i-j)^2 GLCM(i,j)$	*the same to left*	*the same to left*	[14]
	Entropy	$\sum_{i,j=1}^{N_g}(GLCM(i,j))^2$	*the same to left*	*the same to left*	[14]
	Correlation	$\sum_{i,j=1}^{N_g}\frac{\{i\times j\}\times GLCM(i,j)-\{\mu_x-\mu_y\}}{\sigma_x\times\sigma_y}$	*the same to left*	*the same to left*	[14]

Usually, a model with a small number of variables is more interpretable and eliminating irrelevant variables might improve the predictive power [21,54]. Therefore, it is necessary to optimize the number of features for the RF model. When using the RF algorithm to select and optimize variables in remote sensing classifications or regressions, the authors usually used the non-recursive feature elimination (NRFE) algorithm to measure the importance of variables [17,21,26,55,56], since the NREF algorithm was the default method in the random Forest (rfcv function) and varSelRF (varSelRF function) package in R. NREF consists in computing the permutation importance only at the initialization of the algorithm and then following a backward strategy according to this "static" ranking (Table 5). As a consequence, the importance values of the most discriminating correlated variables are not necessarily higher than a less discriminating one, which was demonstrated by Gregorutti et al. (2017) [54] using theoretical analysis and numerical experiments. Relatively, the recursive feature elimination (RFE) algorithm recomputes the permutation importance measures at each step of variable elimination (Table 5). Consequently, it might select a smaller size and more efficient feature subset than NRFE, since the most informative variables are well ranked in the last few steps of the backward procedure, even if they are correlated [54]. The RFE and NRFE methods might obtain a slightly varied features subset every time due to different training sets. Hence the authors employed and replicated the RFE algorithm 20 times to obtain the optimal number of features and compared its performance with the results of NRFE that was also run 20 times. The reiteration time of 20 was enough to select credible and robust feature subsets, which was also recommended by Li et al. (2016) [55]. During each run, the minimum number of variables whose error rate was within one standard error of the minimum cross validation error (referred to as 1 s.e. rule) was chosen as the optimal value. Finally, the most frequent occurrence number and the corresponding features were selected as the optimal number and features, respectively. The RFE and NRFE algorithms were implemented in varSelRF package in R.

Table 5. The processes of non-recursive feature elimination (NRFE) and recursive feature elimination (RFE) algorithms for variable selection.

NRFE	RFE
1. Train an initial random forest model, and rank the features using the permutation importance measure	1. Train a random forest model
2. Eliminate the less relevant feature(s)	2. Compute the permutation importance measure
3. Train a random forest model	3. Eliminate the less relevant feature(s)
4. Repeat steps 2 and 3 until no further features remain	4. Repeat steps 1–3 until no further features remain

After obtaining optimal features, these selected features were input to random forest classification model. Using random forest classification, there are two parameters that need to be tuned: ntree and mtry. The ntree parameter is used to control the maximum number of decision trees to be generated, and the mtry parameter controls the number of variables to be selected for the best split at each node of the trees. Regarding mtry, Rodriguez et al. (2012) [57] recommended setting a relatively small value to avoid generating large generalization errors and reduce the links between individual trees. The mtry parameter was tuned with the starting mtry value of two with intervals of one. Hence, a series of mtry (2, 3, 4, . . . , n) parameters were examined with the ntree value of 1000. Based on the most frequent occurrence of mtry that obtained the lowest OOB error after running the randomForest function 20 times [21], an mtry value of two (15 times), five (8 times), six (10 times) was selected for L8, S2, and P1 data, respectively. Usually, the optimal ntree value is the one that begins to make the OOB error low and convergent [21]. Therefore, in the case where mtry was set to the above optimal value, the authors tested a series of ntree values from 100 to 1000 with intervals of 50. Finally, an optimal value of 500, 800, and 400 was acquired for L8, S2, and P1 data, respectively.

2.7. Accuracy Assessment

Following mangrove extent and species classifications, the overall classification accuracy, the producer's accuracy, and the user's accuracy generated from the confusion matrix were used to assess the accuracy. Furthermore, McNemar's test was utilized to examine whether there was a statistically significant difference between L8, S2, and P1 data in mangrove species classifications. McNemar's test is a non-parametric test based on the binary error matrices of classifier, determining if the classification results using a imagery are equal to those of another imagery (null hypothesis) [58]. The equation for McNemar's test is as follows:

$$z = \frac{f_{12} - f_{21}}{\sqrt{f_{12} + f_{21}}} \tag{5}$$

where, the square of z follows a chi-squared (χ) distribution with 1 degree of freedom, and f indicates the classification frequency expressed in Table 6.

Table 6. Assessment of the statistically significant difference between two classifications using McNemar's test.

		Classifier A	
		Correct	**Incorrect**
Classifier B	Correct	f_{11}	f_{12}
	Incorrect	f_{21}	f_{22}

3. Results

3.1. Mangrove and Non-Mangrove Classification

3.1.1. Visual Examination

The resultant mangrove extent maps of the Dongzhaigang mangrove forest produced from L8, S2, and P1 imagery are shown in Figure 3. The mangrove extent map produced by means of field survey and manual visual interpretation in 0.5-m pan-sharpened P1 imagery is presented in Figure 3D, which is used as a reference map. Using visual overview, all three data extracted the mangrove extent overall, with the major difference among the three maps on the west side of the DNNR. The map produced by P1, for that area, had a lot of misclassified mangrove patches, as did L8 and S2, but their errors were fewer. Within DNNR, the L8, S2, and P1 classifications could precisely extract the mangrove areas, with an area of 1461 ha, 1436 ha, and 1363 ha, respectively, of which the map produced by L8 had the smallest discrepancy from that of visual interpretation. The mangrove area within DNNR produced by the visual interpretation and field survey in 2014 is 1548 ha. Additionally, compared with L8 and S2, though the map produced by the very high spatial resolution P1 imagery could better render the creeks within the mangrove forests, the mangroves along the creeks were underestimated. Relatively, for the landward-edge mangrove forests, the performance of P1 did not exceed that of L8 and S2.
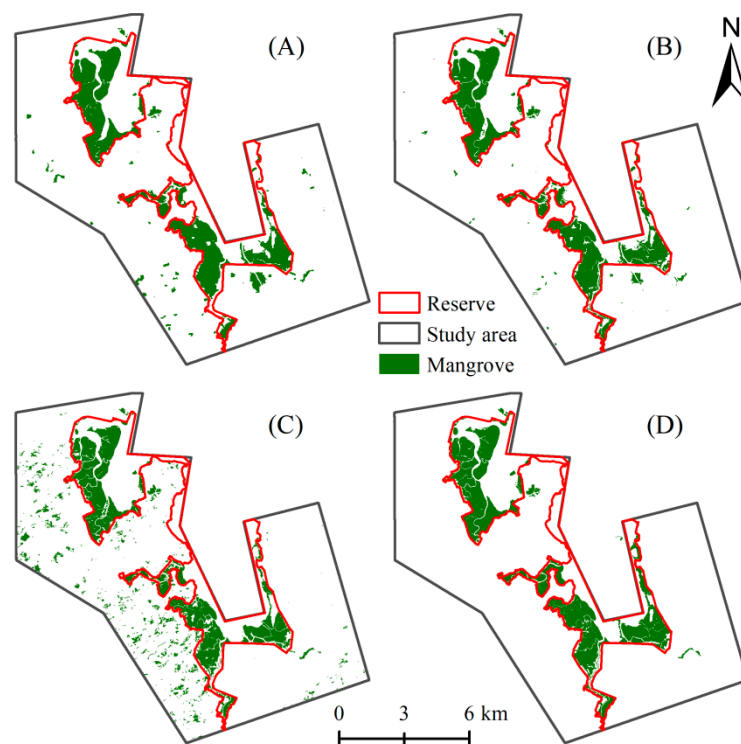
Figure 3. Comparison of (**A**) Landsat 8, (**B**) Sentinel-2, (**C**) Pléiades-1, and (**D**) manual visual interpretation based on field survey using Pléiades-1 image for mangrove extent classifications.

3.1.2. Accuracy Assessment

The classification accuracy of vegetation cover types using the S2, L8, and P1 data is shown in Table 7. They were assessed by 512 pre-prepared validation samples, respectively, which was randomly produced within the corresponding vegetation mask generated at level 1 in ArcGIS 10.2 and visually interpreted in P1, S2, images and Google Earth images. The overall accuracy of mangrove and non-mangrove classifications using L8, S2, and P1 were 96.09%, 96.52%, and 91.89%, respectively. Regarding the user's accuracy, the mangroves were similar between L8 and S2, both reaching about 90%, while for P1 the mangrove user's accuracy was the lowest with an accuracy of only 72.93%, indicating that there were many incorrect classifications in the mangrove objects presented in Figure 3C. Discussing terms of the producer's accuracy for mangrove classification, P1 had highest accuracy (94.17%), followed by L8 (92.66%), and S2 (90.29%), which implied that the resultant map produced by S2 had the largest number of mangroves that were misclassified as non-mangrove vegetation.

Table 7. Accuracy descriptive statistics of vegetation cover type level.

Class	Landsat 8, 15 m				Sentinel-2, 10 m				Pléiades-1, 0.5 m			
	Pa	Ua	Oa	K	Pa	Ua	Oa	K	Pa	Ua	Oa	K
Mangrove	92.66	89.38	96.09	0.93	90.29	92.08	96.52	0.94	94.17	72.93	91.89	0.87
Non-mangrove	97.02	97.99			98.07	97.60			91.33	98.44		

Pa. producer's accuracy, Ua: user's accuracy, Oa: overall accuracy, and K: Kappa.

3.2. Object Feature Selection for the RF Model on Species Discrimination

Subsequent to running the RFE and NRFE algorithms 20 times, the authors obtained the averaged OOB error versus the number of features and the optimal number of features (Figure 4). During the experiment, mtry was set to the square of the number of mtry, and the number of trees used for the first forest and the others was 5000 and 2000, respectively. Concerning the three satellite data, the OOB

error decreased faster for RFE than for NRFE, which indicated that RFE provided an efficient screening of the features overall. This superiority of RFE was obvious in small-size models, such as 6, 7, 8, and 9. Regarding L8, S2, and P1 data, the optimal number of classification features was eight (15 times), nine (9 times), and eight (16 times) using the RFE algorithm, respectively. Relatively, when using the NRFE algorithm, the numbers were nine (12 times), twelve (8 times), and ten (8 times) for L8, S2, and P1 data, respectively.

Looking at the L8 data with the optimal number of eight (8/126) features, the mean OOB error was 25.88% for NRE, while it was 26.48% for NRFE. Studying the S2 data with the optimal number of nine (9/218) features, the mean OOB error was 24.27% for NRE, while it was 25.93% for NRFE. Examining the P1 data with the optimal number of eight (8/73) features, the mean OOB error was 18.52% for NRE, while it was 24.45% for NRFE. Furthermore, the optimal features selected by NRFE used more features and produced slightly higher OOB errors than that of RFE. Generally, the results showed that the screening of the optimal features proposed by NRF were superior to that of NRFE, especially for the P1 data. Finally, the top eight, nine, and eight features with the most frequent occurrence were used in the final RF classification models for L8, S2, and P1 data, respectively.
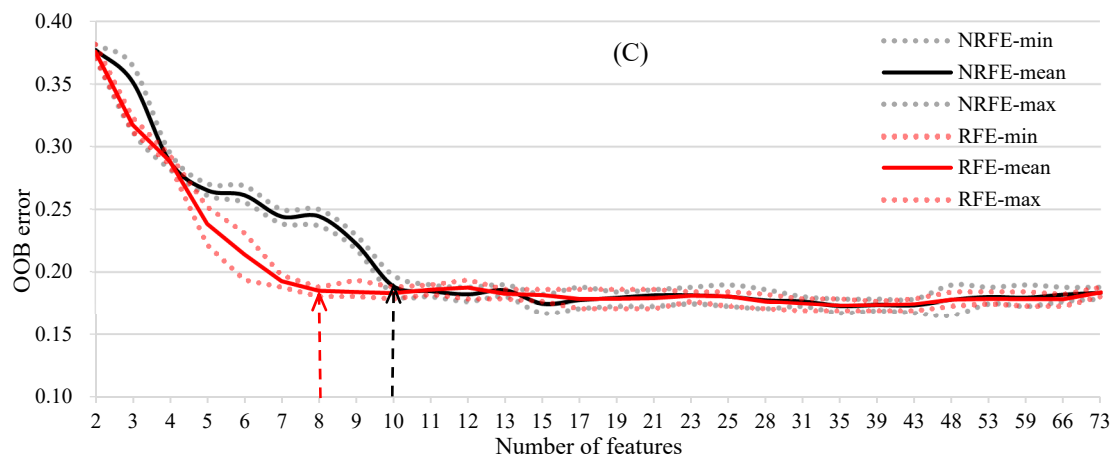

Figure 4. *Cont.*

Figure 4. The out-of-bag (OOB) error estimate versus the number of features used for RFE and NRFE algorithms based on 20 runs: (**A**) Landsat 8; (**B**) Sentinel-2; and (**C**) Pléiades-1.

3.3. Feature Importance for Species Discrimination

Subsequent to optimizing the feature space and tuning the ntree and mtry parameters, the relative importance of the input features was measured for L8, S2, and Pl data, respectively (Figure 5). Regarding L8 imagery, shortwave infrared (SWIR) B6 and B7 were the most important bands for mangrove species classifications, followed by aerosol band B1 and near-infrared band B5. The MDI1 computed from B6 and EVI computed from B5 were the top five features in the variable importance ranking. Studying the S2 dataset, red edge bands were the most informative variables in demarcating mangrove species, followed by shortwave infrared and near infrared bands. Red edge B5, and its derived CIre1 and NDVIre1 indices, ranked first, third, and fourth, respectively, and the shortwave infrared B11 was the second most important feature, for example. Additionally, red edge B6 and its derived index CIre2 were also selected in S2 models, ranking seventh and sixth, respectively, which further demonstrated red edge bands were paramount for mangrove species classifications. Concerning the P1 image, the most important three features were EVI, GLCM Correlation b4 in 0° direction, and blue B1, which was different from that of the L8 and S2 models. It was the first time that texture information features appeared and ranked top two in the classification model.
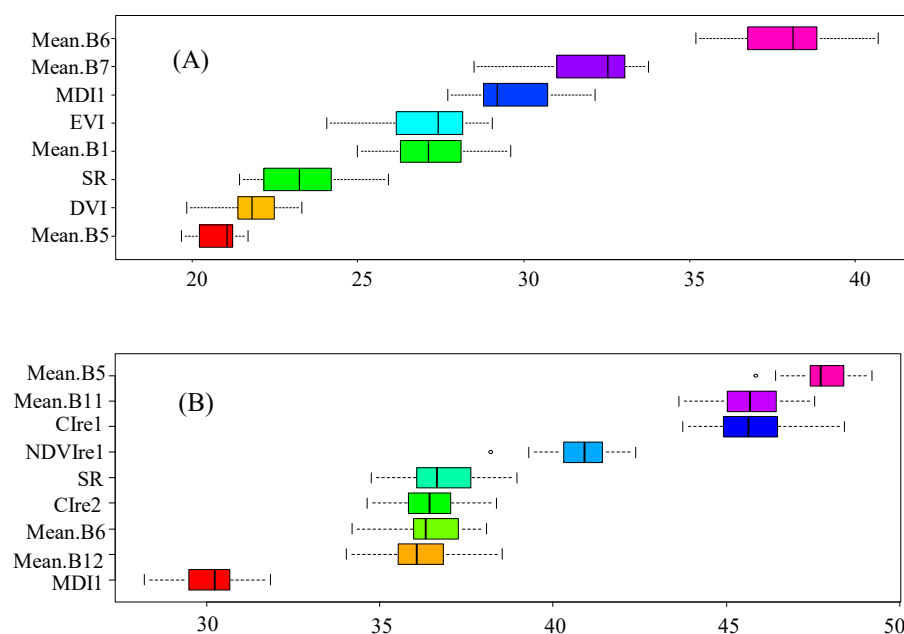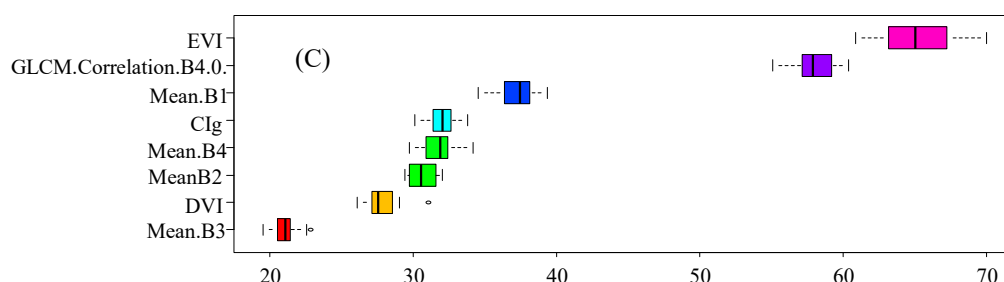

Figure 5. *Cont.*

Figure 5. Ranking of image features based on the importance measure by %InSE (the percentage increase in the standard error) obtained from 20 runs of the RF for: (**A**) Landsat 8; (**B**) Sentinel-2; and (**C**) Pléiades-1.

3.4. Mangrove Species Community Classification

3.4.1. Visual Examination

In order to ensure a relative fairness of level three classifications (namely, within a true mangroves mask of each image), we visually checked the mangrove polygons and corrected obvious errors inherent in the mangrove extent map before the level three classification. The resultant mangrove species community maps of the Dongzhaigang mangrove forest produced from L8, S2, and P1 imagery are shown in Figure 6. Using visual overview, the three thematic maps all portrayed that the north of the study area was mainly covered by *R. stylosa* and *C. tagal*, while in the south *B. sexangula* was the dominant mangrove species. The major visual difference interpreted between the three thematic maps were in areas I, II, and III (Figure 6).
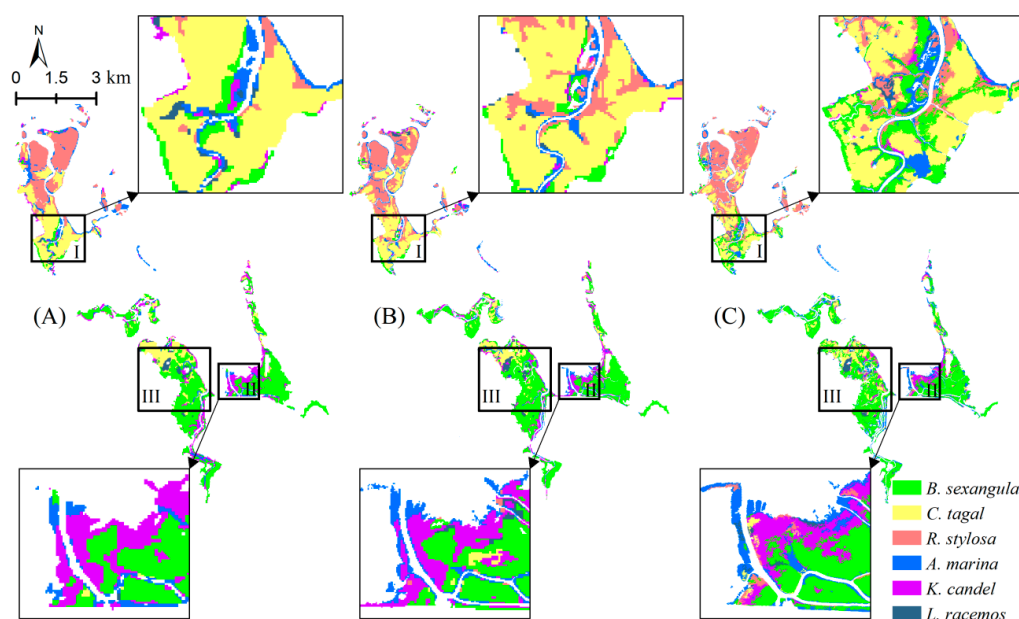

Figure 6. Comparison of (**A**) Landsat 8, (**B**) Sentinel-2, and (**C**) Pléiades-1 imagery for mangrove species community classifications.

Studying area I, the three thematic maps all presented *A. marina* on the left side of the estuary, but the visual amount in the P1 and L8 produced maps was higher than that in S2. Examining the right side of the estuary, the S2 and P1 classifications appeared to show strip *R. stylosa*, whereas the map produced by L8 was only covered with two patches of *R. stylosa*. Scrutinizing the south of the river in area I, *B. sexangula* was obviously displayed on both sides of the river in the map produced by the P1 image, while the map produced by S2 showed that there was still *C. tagal* and the map of L8 presented

a few of the *B. sexangula* and *A. marina*. Through a visual comparison with the field survey data and the 0.5-m P1 image, the authors found that on the fringe of the river *B. sexangula* was the dominant species, which indicated that the P1 based classification was more consistent with the actual mangrove species. Looking at area II, all the three maps depicted *K. candel* seaward, but the visual amount of *K. candel* in the S2 produced map was less than that of L8 and greater than that of P1. Compared with the P1 image and field survey data, the authors found that *K. candel* in the map produced by P1 imagery was more precise, which implied that the S2 and L8 classifications overestimated *K. candel*, especially for the L8 classification. Area III was the most intricate area of mangrove species communities. The difference between S2 and L8 classifications in area III was relatively small, and the map produced by P1 imagery was dotted with more amount of *K. candel* and *C. tagal* patches, which was noticeably different from the maps of S2 and L8.

3.4.2. Accuracy Assessment

The classification accuracy of the mangrove species community using different imagery is shown in Table 8 and the statistically significant comparison through McNemar's test is presented in Table 9. Generally, the overall classification accuracy was positively correlated with the spatial resolution of the imagery in the study area. The resultant classification using 0.5-m P1 imagery had the highest accuracy (78.57%), followed by 10-m S2 imagery (70.95%), and 15-m L8 imagery (68.57%). By comparison with the classification models that all features were used to train the RF algorithm (ntree = 1000, mtry = $\sqrt{\text{number of variables}}$), the overall accuracies of S2, L8, and P1 increased by 3.81%, 2.55% and 0.48%, respectively.

Discussing the producer's accuracy, the accuracies of *B. sexangula*, *R. stylosa*, and *L. racemosa* were positively correlated with the image spatial resolution, and they were well classified. The producer's accuracy of *B. sexangula*, for example, improved from 75.00% in L8 to 93.75% in P1. The producer's accuracy of *K. candel* was the lowest in all mangrove species types, which indicated that more than 50% of *K. candel* was misclassified as other species. *A. marina* was a type of pioneer mangrove species and occasionally grew on the fringe of water in the study area. It had low producer's accuracy in the map generated from L8 and S2 imagery, but in the P1 derived map, more than 3/4 of *A. marina* were classified correctly. The producer's accuracy of *C. tagal* was relatively stable in the three thematic maps with an accuracy ranging from 60.42% to 66.67%. Reviewing the user's accuracy, the accuracies of all six types of mangrove species were correlated almost positively with the spatial resolution. *L. racemosa*, with the highest user's accuracy, increased from 82.35% to 90.91%, and *K. candel*, with the lowest user's accuracy, increased from 50.00% to 66.67%, which were consistent with the above visual examinations and indicated that the *K. candel* objects had many misclassified patches from other mangrove species. The two dominant species *C. tagal* and *R. stylosa* rose from 63.04% and 75.47%, to 74.42% and 83.67%, respectively.

When comparing the mangrove species classification of S2 with those of L8 and P1, McNemar's test manifested the observed difference of the S2 and L8 derived classifications, which was not statistically significant (p = 0.05), while the S2 derived classification was statistically lower in significance than that of P1 (p = 0.05).

Table 8. Accuracy descriptive statistics of mangrove species at community level.

Class	Landsat 8				Sentinel-2				Pléiades-1			
	Pa (%)	Ua (%)	Oa (%)	K	Pa (%)	Ua (%)	Oa (%)	K	Pa (%)	Ua (%)	Oa (%)	K
B. sexangula	75.00	66.67			81.25	68.42			93.75	73.77		
C. tagal	60.42	63.04			66.67	68.09			66.67	74.42		
R. stylosa	79.17	79.17	68.57	0.66	83.33	75.47	70.95	0.68	85.42	83.67	78.57	0.76
K. candel	50.00	52.38			40.91	50.00			45.45	66.67		
A. marina	72.27	66.67			50.00	78.57			77.27	85.00		
L. racemosa	63.64	82.35			81.82	85.71			90.91	90.91		

Pa: producer's accuracy, Ua: user's accuracy, Oa: overall accuracy, K: Kappa.

Table 9. Statistically significant comparison between Landsat 8, Sentinel-2, and Pléiades-1 in mapping mangrove species.

	McNemar's Test chi-Square	*p*-Value
Sentinel-2 vs. Landsat 8	0.3636	0.54650
Sentinel-2 vs. Pléiades-1	4.7407 *	0.02946 *
Landsat 8 vs. Pléiades-1	8.3333 *	0.00389 *

The symbol "*" indicates that the difference is statistically significant because the p value is below the critical value of 0.05.

4. Discussion

4.1. The Potential of Sentinel-2 Data for Mangrove Extent and Species Classifications

How to select an optimal and cost-effective remote sensing image and develop an efficient classification framework, for mangrove forests inventories in a required scale, which is of concern to mangrove managers, ecologists, and geographers. This study explored the strength of the newly-launched and freely-available Sentinel-2 sensor in mapping mangrove extent and species regarding its extra red-edge bands and refined spatial resolution, using the three-level geographic object-based image analysis and a machine learning algorithm in Dongzhaigang, Hainan, China. The results were compared with those derived using the freely-available Landsat 8 and the commercial Pléiades-1 imagery. The study demonstrated that, at the mangrove extent scale, S2 and L8 could precisely discriminate mangrove from terrestrial vegetation and the overall classification accuracies of L8 and S2 were higher than that of P1, which was contradictory to the general reasoning in terrestrial vegetation classifications that the higher the resolution, the greater the accuracy [59]. The reason may be that the well pan-sharpened image (Landsat 8) and the more spectral bands (Landsat 8 and Sentinel-2) in moderate sensors could improve the information extraction. Heenkenda et al. (2014) [13] have demonstrated that pan-sharpened WorldView-2 imagery has significantly higher accuracy than non pan-sharpened WorldView-2 imagery and 0.14-m aerial photographs in mapping mangrove species. Looking at species on a community scale, S2 and L8 could only extract accurately about 70% of mangroves, and the overall accuracy of P1 was higher than that of S2, followed by L8, which was consistent with the conclusions of Shoko and Mutanga (2017) [25] and Ng et al. (2017) [56] in other vegetation species classifications. The former study found that the S2 sensor produced higher overall classification accuracies than the L8 sensor in discriminating C3 and C4 grass species; the latter research proved that the P1 imagery outperformed S2 for the detection of two terrestrial trees. However, with respect to statistical analysis by McNemar's test, there was no statistically significant difference between S2 and L8 sensors at mangrove species community scales.

The only uncertainties introduced in the accuracy comparison were attributed to the two years gap between the 2014 image (Pléiades-1) and two 2016 images (Sentinel-2 and Landsat 8). In the early 2017 field survey, we found that several samples had been devastated by natural factors such as typhoon, in comparison with the field survey of 2014. In order to reduce the impact, the authors moved these samples to the same species community nearby, which was stable from 2014 to 2016. Even so, there is some level of changes in mangrove between the two period of images. However, when these changes are placed in the whole mangrove forests, they are tiny. Therefore, the comparison among the three images are still valid. Furthermore, it remains to be seen if forthcoming results using S2 imagery from other countries' or regions' mangrove forests are similar to this study's.

Developing an efficient framework for mapping mangroves requires an understanding of the spectral, physical, and spatial distribution characteristic of the mangroves and surrounding land covers [13,40]. There is no universal framework for different imagery and sites [20,30,40,60]. In the study, we used a modified traditional three-level hierarchical framework for mangrove extent and species mapping in Dongzhaigang, Haikou, China. However, the three images were photographed by different sensors—Sentinel-2A MSI, Landsat 8 OLI, and Pléiades-1B. They have different spectral responses, spatial resolutions, and spectral bands (Table 1). These intrinsic characteristics determine

that different algorithms and thresholding values will be applied to the three images to map similar objects (Table 3). In addition, the framework using the same sensors can not directly transferred to other sites because of different ecological characteristics of mangrove system, climate, and solar altitude angle. A modification of input features and thresholding value may be required. However, the findings of the study may provide a point of reference for the modification or a new construction of the framework.

Therefore, the authors can assert that S2 is capable of mapping mangrove extent. Regarding mangrove species community classification, the application of S2 imagery might be recommended, but it should be cautiously applied, especially in mixed mangrove species regions.

4.2. The Relationship between Spatial Resolutions and Mangrove Features

The outcomes in the current study showed that the moderate spatial resolution sensors S2 and L8 outperformed the very high resolution sensor P1 in mapping mangrove extent (Table 7), while, for mangrove species discriminations, the P1 sensor was superior to S2 and L8 (Tables 8 and 9). These results indicated that spatial resolutions had an important impact on the classifications of mangrove features, but due to the difference of satellite sensors (mainly different in spectral bands), this impact was not simply related to spatial resolutions.

When using the same or similar remote sensors to map mangrove features, Kamal et al. (2014) [59] found that the smaller the pixel size, the more detailed the mangrove features that could be identified based on a series of resampled WorldView-2 images.

However, when using different sensors to map larger mangrove features such as mangrove zonations and extent, the moderate imagery could outperform high resolution imagery with the help of more spectral bands, which was also demonstrated by Shapiro et al. (2015) [28]. Their studies showed that the overall accuracy of WorldView-2 was lower than that of Landsat 8 in mapping mangrove extent [28]. In the study, the overall accuracies of S2 and L8 are also higher than that of P1 for mangrove extent classification (Table 7). The authors created MDI2 utilizing SWIR2 and NIR bands to extract mangrove extent for S2 and L8 imagery, for example, but for P1 could not use MDI2 as it did not have SWIR band (Table 3 and Figure A2). Consequently, the two emerging sensors both can precisely identify mangrove extent with reducing manual inspection and editing work.

Used for mapping small-sized features and internal variations of the mangrove canopy such as foliage clumping, tree crown, and species communities, spatial resolution might be more important than the spectral bands [30,40]. Figure 7 is an illustration of how spatial resolutions affected the identification of mangrove species communities of three typical shapes (point, line and polygon) for L8, S2, and P1 imagery in Dongzhaigang. The authors found that the P1 data could effectively map the spatial distribution of point/line/polygon-shaped mangrove species communities. However, for S2 and L8 data, they over or under-classified the target species to some extent. Regarding Group I, the L8 and S2 sensors resulted in under and over-classification of point shape *A. marina*, respectively. Meanwhile, they both have obvious misclassifications. The under-classification in L8 may be because the spatial extent of mangrove species is less than the pixel size, which leads to the point mangroves being dissolved by mudflats. The over-classification in S2 may be because the mixed reflectance spectra of mangroves, underlying mudflats, waters, and atmospheric vapor in one pixel [13]. The same phenomenon was also encountered in the classification of line shape mangrove (Group II, Figure 7). Concerning homogeneous mangrove species, both moderate and high spatial resolution imagery could well discriminate (Group III-1, Figure 7), whereas, for heterogeneous mangrove species (Group III-2, Figure 7), given to very high spatial resolution, P1 properly mapped *B. sexangula* on the fringe of the river and *R. stylosa* and *K. candel* in the zonation close to sea. The S2 derived classification basically demarcated the mosaic mangrove species community, but the small patch species communities were dissolved within the major surrounding class. This phenomenon was more likely to happen in the L8 classification, as presented in Group III-2 in Figure 7.
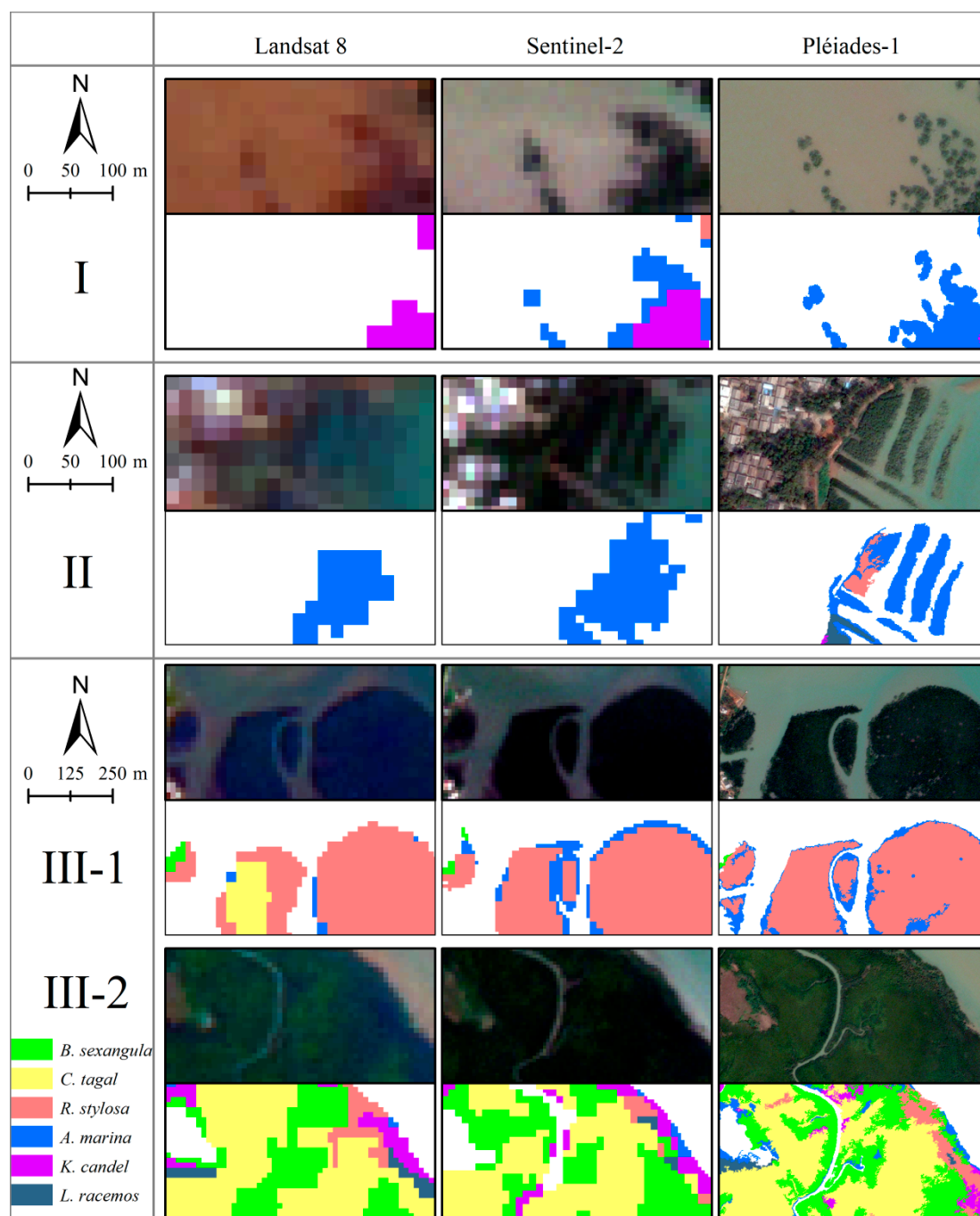
Figure 7. Examples of point (I), line (II) and polygon (III) mangrove classifications using the Landsat 8, Sentinel-2, and Pléiades-1 imagery in Dongzhaigang. Group III-1 is an area of homogeneous mangrove species communities, and Group III-2 is an area of heterogeneous mangrove species communities.

4.3. The Importance of Spectral Bands and Texture Information for Mangrove Classifications

The above, Section 4.2, discussed that the added spectral bands could help moderate sensors map large mangrove features. When separating vegetation from other landscapes in this study, the authors created and used WFI; when demarcating mangroves from terrestrial vegetation, the authors created and utilized MDI2. The two newly invented indices were computed from the SWIR-2 and NIR band. Shi et al. (2016) [61] also used SWIR-2 and SWIR-1 band-derived indices to enhance the spectral differences of mangrove forests and terrestrial vegetation based on L8 imagery. Chen et al. (2017) [18] employed NDVI, EVI, and LSWI (land surface water index, computed from NIR and SWIR bands) to

map the total mangrove forests in China. Compared with terrestrial vegetation, mangroves grow in inter-tidal regions and are inundated by periodic seawater, so the shortwave infrared reflectance of mangroves is lower than that of terrestrial vegetation (Figure A2). Consequently, the authors asserted that the shortwave infrared bands were imperative for mangrove extent classification, followed by the NIR band.

Considering the mangrove species scale, the functions of NIR, SWIR and red edge bands were also different, as were the indices derived from them. Above all, the features selected in the RFE algorithm were more important than the unselected features.

Regarding L8, the classification model showed that the top three important features were related to SWIR. The NIR and red related features were selected as five (5/8) and three (3/8) times, respectively. However, when Shoko and Mutanga (2017) [25] used L8, S2, and WorldView-2 to discriminate C3 and C4 terrestrial grass, they showed that red band was the most important, followed by NIR. There was an evident discrepancy between mangrove species classification and terrestrial vegetation classification in utilizing L8 data. Concerning S2, the result portrayed that red-edge related features were used five (5/9) times, followed by SWIR (three times, 3/9) and NIR (three times, 3/9). Meanwhile, the red-edge related features were overall ranked higher than that of SWIR, and the SWIR features higher than the NIR features. Since there was no literature on mangrove species classification using S2 data and measuring the importance of spectral features, the authors could not verify the results, but Wang et al. (2009) [62] had assessed the contribution of narrow red, red-edge, NIR, and SWIR bands to the mangrove species classification based on laboratory measurements of hyperspectral leaf reflecting. Their results proved that the descending order of spectral contributions is red-edge, SWIR, NIR, and red bands. The current findings were consistent with their conclusions. Discussing the discriminations of terrestrial vegetation, Shoko and Mutanga (2017) [25] showed that the red-edge band was the most influential, followed by blue, SWIR, red bands, and NIR bands. Ng et al. (2017) [56], however, said NIR, green, and blue bands were the most important bands in demarcating *Prosopis* and *Vachellia* spp, based on S2 data. These studies manifested that the importance of spectral bands of S2 sensor was varied, and the red-edge bands were not always the most important for vegetation classifications. Looking at P1, the outcome indicated that the NIR related features were utilized five times (5/8), followed by red-related features (three times, 3/8). Examining the original spectral bands only, the blue band was the most important. The blue band was also found to be vital in discriminating *Prosopis* and *Vachellia* spp based on the same P1 sensor [56]. Through synthesizing the above analyses, Figures 5 and A3, the authors reasoned that, at the mangrove species community scale, the most important feature, overall, is red-edge band, followed by SWIR, NIR, blue, and other visual bands in turn.

The texture features were useful in mapping mangrove species, as described in References [14,15,20]. Using the three optimal tuning models, only P1 employed texture feature—GLCM Correlation b4 (0° direction). The reason might be that only the high spatial resolution of the image could reflect texture information discrepancies of different mangrove species communities and the spatial resolutions of L8 and S2 were too coarse.

4.4. The Superiority of Random Forests Classification

Over the last two decades, the random forest algorithm has received increasing attention due to the excellent classification results and the easy building model [42,50,63]. Compared with other state-of-the-art machine learning algorithms, RF was more robust and stable to the variation of segmentation scales, the selection of object features and the parameter configuration [52,64], but it was more sensitive to the sample design and training set size [50,52]. Colditz (2015) [65] found that area-proportional allocation of training samples per class outperformed the allocation of an equal number of samples to each class and the allocation of random sampling in RF classification. Considering this information, the authors used a different number of samples for per mangrove species (Table 2) and the three dominant species were allocated more samples.

Furthermore, the RF algorithm can quantitatively measure the importance of input features and optimize feature space. Breiman (2001) [51] described that when there were a lot of correlated features in the RF model, these correlated features would have more chance to be selected in trees and makes the correlation between the individual trees become higher, consequently leading to the generalization ability of the RF model being weak. The authors assumed that not all the features were relevant for mangrove species classification and some irrelevant features might have a negative effect on the models accuracy. Regarding the stage of feature space optimization, this assumption was proven, since the OOB errors of L8 and S2 classification models using all the input features (126 and 218, respectively) were obviously higher than those of the models using an optimal number of features (Figure 4). Furthermore, the overall classification accuracies of S2, L8, and P1 using the optimal features all improved in comparison with the classification models that all features were used to train RF algorithm. The largest growth happened in the S2 model (3.18%), which initially had the highest number of input features, followed by L8 (2.55%), and P1 (0.48%). These results conclude that the RFE algorithm is more efficient in screening large variables model. The reason why the increments are not obvious may be that ntree is set to 1000 for all the features inputted into models, which is high enough for the RF trees to grow and handle high dimensional datasets [21,52]. Were the authors to still directly use the RF algorithm to measure feature importance and select the top *n* features, or utilized the NRFE algorithm, as a lot of studies showed [21,56], it would lead to incorrect model interpretation and a misleading feature ranking [66]. Alternatively, the RFE algorithm could solve this problem through recomputing the permutation importance measures at each step of variable elimination. Gregorutti et al. (2017) [54] explained how correlated variables affected important ranking and feature selection, and demonstrated that RFE was superior to NREF in classifying land cover based on Landsat satellite dataset.

5. Conclusions

This study evaluated the performance of the freely-available and newly-launched Sentinel-2 (S2) sensor and compared it with that of the Landsat 8 (L8) and the Pléiades-1(P1) in classifying and mapping two scales of mangrove features: Mangrove extent and mangrove species communities. It is the first study dedicated to examining the potential of original spectral bands, spectral indices, and texture information of S2 for mangrove feature classifications. Based on the current findings, the authors conclude that:

(1) The modified three-level hierarchical classification framework corresponded to the ecosystem structure of mangrove forests and could help to clearly map mangrove features of different scales in use of S2, L8, and P1 imagery.

(2) At mangrove extent scale, the S2 and L8 imagery could accurately extract mangrove stands with both the producer's accuracy and user's accuracy reaching about 90%, while the 0.5-m P1 imagery obviously overestimated mangrove stands with a user's accuracy of only 72.93%. The high accuracies of the S2 and L8 sensors were attributed to the shortwave infrared bands.

(3) At mangrove species communities scale, the overall classification accuracy of S2 was 70.95%, which was lower than P1 imagery (78.57%) and better than L8 data (68.57%). Though the overall accuracies were moderate, some individual classes had higher accuracies. Both *R. stylosa* and *L. racemosa* had over 80% accuracy in P1, and over 75% in S2. Regarding the other two dominant species, *B. sexangula* and *C. tagal*, the S2 and P1 data could identify their major characteristics with accuracies of more than two-thirds. The accuracy of pioneer and fringe *A. marina* differed among the three sensors, and the moderate imagery could not identify it well. The occasionally distributed *K. candel* always had the lowest accuracy, which meant it was hard to demarcate in the study area. When the three thematic maps, produced by different imagery, were compared by McNemar's test, the classification accuracy of S2 was statistically different from P1 (*p* = 0.05), but not statistically different from L8.

(4) The recursive feature elimination (RFE) algorithm provided a more efficient screening of features than did the non-recursive feature elimination (NRFE) algorithm, faced with high-dimension

and correlated variables. Using L8, S2, and P1 data, the optimal number of species community classification features was eight (8/126), nine (9/218), and eight (8/73), respectively. Considering feature importance, red-edge bands were the most informative variables in demarcating mangrove species, follow by SWIR and NIR bands in S2 data. Discussing L8 and P1 imagery, SWIR-1 and EVI (enhanced vegetation index) were the most important features, respectively. Meanwhile, only P1 employed a textured feature—GLCM Correlation b4 (0° direction) that ranked second—which indicated the texture information of moderate spatial resolution imagery could not capture the discrepancies of different mangrove species communities.

The obtained findings have demonstrated the potential of the S2 imagery as a valuable data source for mapping different scales of mangrove features. Multi-temporal S2 imagery might be an alternative solution to improve accuracy in the future, with the continuous acquisition of binary S2 satellites.

Conflicts of Interest: The authors declare no conflict of interest.

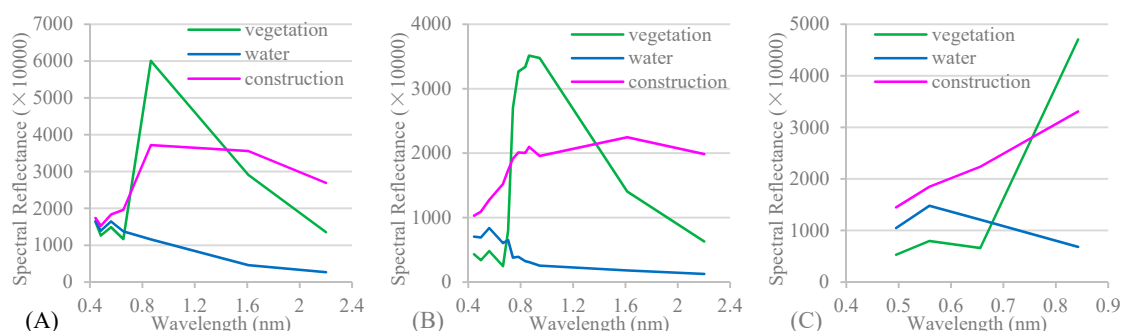## Appendix A. The spectral reflectance used in Level 1, Level 2 and Level 3

Figure A1. The spectral reflectance of vegetation, water and construction (construction land, mudflat and bare land) in (**A**). Landsat 8, (**B**). Sentinel-2 and (**C**). Pléiades-1 in level 1, which was produced based on 50 representative samples per class.
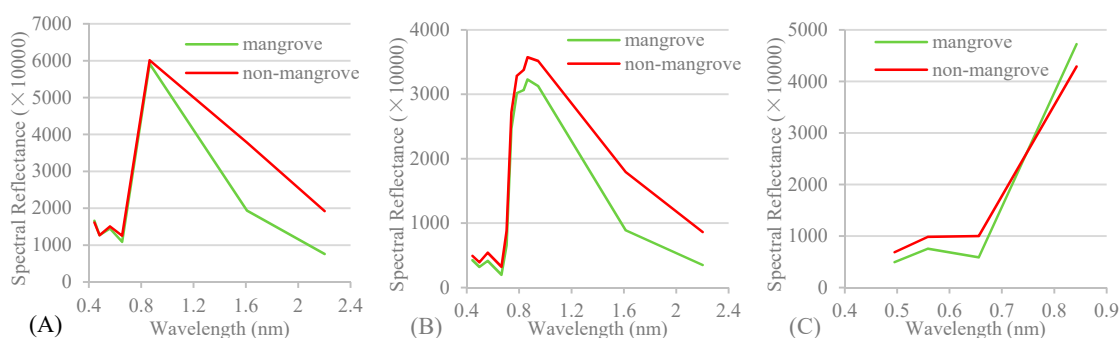

Figure A2. The spectral reflectance of mangroves and non-mangroves in (**A**). Landsat 8, (**B**). Sentinel-2 and (**C**). Pléiades-1 in level 2, which was produced based on 60 representative samples per class.
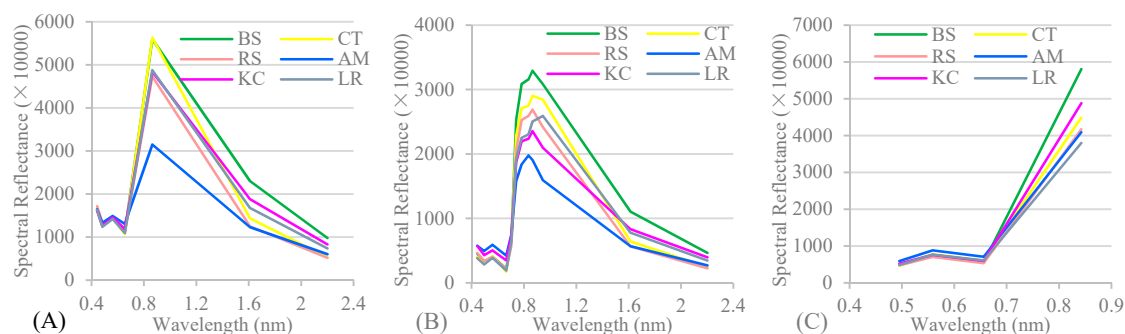
Figure A3. The spectral reflectance of six mangroves species in (**A**). Landsat 8, (**B**). Sentinel-2 and (**C**). Pléiades-1 in level 3. BS is *B. sexangula*, CT is *C. tagal*, RS is *R. stylosa*, KC is *K. candel*, AM is *A. marina*, and LR is *L. racemos*.

References

1. Giri, C.; Ochieng, E.; Tieszen, L.L.; Zhu, Z.; Singh, A.; Loveland, T.; Masek, J.; Duke, N. Status and distribution of mangrove forests of the world using earth observation satellite data. *Glob. Ecol. Biogeogr.* **2011**, *20*, 154–159. [CrossRef]
2. Giri, C. Observation and monitoring of mangrove forests using remote sensing: Opportunities and challenges. *Remote Sens.* **2016**, *8*, 783. [CrossRef]
3. Duke, N.C.; Meynecke, J.O.; Dittmann, S.; Ellison, A.M.; Anger, K.; Berger, U.; Cannicci, S.; Diele, K.; Ewel, K.C.; Field, C.D. A world without mangroves? *Science* **2007**, *317*, 41. [CrossRef] [PubMed]
4. Baowen, L.; Qiaomin, Z. Area, distribution and species composition of mangroves in china. *Wetl. Sci.* **2014**, *12*, 435–440. (In Chinese)
5. Kuenzer, C.; Bluemel, A.; Gebhardt, S.; Tuan Vo, Q.; Dech, S. Remote sensing of mangrove ecosystems: A review. *Remote Sens.* **2011**, *3*, 878–928. [CrossRef]
6. Heumann, B.W. Satellite remote sensing of mangrove forests: Recent advances and future opportunities. *Prog. Phys. Geog.* **2011**, *35*, 87–108. [CrossRef]
7. Long, J.B.; Giri, C. Mapping the philippines' mangrove forests using landsat imagery. *Sensors* **2011**, *11*, 2972–2981. [CrossRef] [PubMed]
8. Jia, M.; Wang, Z.; Li, L.; Song, K.; Ren, C.; Liu, B.; Mao, D. Mapping china's mangroves based on an object-oriented classification of landsat imagery. *Wetlands* **2014**, *34*, 277–283. [CrossRef]
9. Mondal, P.; Trzaska, S.; de Sherbinin, A. Landsat-derived estimates of mangrove extents in the sierra leone coastal landscape complex during 1990–2016. *Sensors* **2018**, *18*, 12. [CrossRef] [PubMed]
10. Kuenzer, C.; van Beijma, S.; Gessner, U.; Dech, S. Land surface dynamics and environmental challenges of the niger delta, africa: Remote sensing-based analyses spanning three decades (1986–2013). *Appl. Geog.* **2014**, *53*, 354–368. [CrossRef]
11. Jia, M.M.; Liu, M.Y.; Wang, Z.M.; Mao, D.H.; Ren, C.Y.; Cui, H.S. Evaluating the effectiveness of conservation on mangroves: A remote sensing-based comparison for two adjacent protected areas in shenzhen and hong kong, china. *Remote Sens.* **2016**, *8*, 627. [CrossRef]
12. Zhang, X.H.; Treitz, P.M.; Chen, D.M.; Quan, C.; Shi, L.X.; Li, X.H. Mapping mangrove forests using multi-tidal remotely-sensed data and a decision-tree-based procedure. *Int. J. Appl. Earth. Obs. Geoinf.* **2017**, *62*, 201–214. [CrossRef]
13. Heenkenda, M.; Joyce, K.; Maier, S.; Bartolo, R. Mangrove species identification: Comparing worldview-2 with aerial photographs. *Remote Sens.* **2014**, *6*, 6064–6088. [CrossRef]
14. Wang, T.; Zhang, H.; Lin, H.; Fang, C. Textural–spectral feature-based species classification of mangroves in mai po nature reserve from worldview-3 imagery. *Remote Sens.* **2016**, *8*, 24. [CrossRef]
15. Dezhi, W.; Bo, W.; Penghua, Q.; Yanjun, S.; Qinghua, G.; Xincai, W. Artificial mangrove species mapping using pléiades-1: An evaluation of pixel-based and object-based classifications with selected machine learning algorithms. *Remote Sens.* **2018**, *10*, 294.

16. Castillo, J.A.A.; Apan, A.A.; Maraseni, T.N.; Salmo, S.G. Estimation and mapping of above-ground biomass of mangrove forests and their replacement land uses in the philippines using sentinel imagery. *ISPRS J. Photogramm. Remote Sens.* **2017**, *134*, 70–85. [CrossRef]

17. Zhu, Y.; Liu, K.; Liu, L.; Myint, S.; Wang, S.; Liu, H.; He, Z. Exploring the potential of worldview-2 red-edge band-based vegetation indices for estimation of mangrove leaf area index with machine learning algorithms. *Remote Sens.* **2017**, *9*, 1060. [CrossRef]

18. Chen, B.Q.; Xiao, X.M.; Li, X.P.; Pan, L.H.; Doughty, R.; Ma, J.; Dong, J.W.; Qin, Y.W.; Zhao, B.; Wu, Z.X.; et al. A mangrove forest map of china in 2015: Analysis of time series landsat 7/8 and sentinel-1a imagery in google earth engine cloud computing platform. *ISPRS J. Photogramm. Remote Sens.* **2017**, *131*, 104–120. [CrossRef]

19. Leon, T.; Giang, V.; An, B.; Minh, N.; Quynh, N.T.; Le, Q.; Viet, P. Uncovering the spatio-temporal dynamics of land cover change and fragmentation of mangroves in the ca mau peninsula, vietnam using multi-temporal spot satellite imagery (2004–2013). *Appl. Geog.* **2017**, *86*, 197–207.

20. Wang, L.; Sousa, W.P.; Peng, G.; Biging, G.S. Comparison of ikonos and quickbird images for mapping mangrove species on the caribbean coast of panama. *Remote Sens. Environ.* **2004**, *91*, 432–440. [CrossRef]

21. Pham, L.T.H.; Brabyn, L. Monitoring mangrove biomass change in vietnam using spot images and an object-based approach combined with machine learning algorithms. *ISPRS J. Photogramm. Remote Sens.* **2017**, *128*, 86–97. [CrossRef]

22. Drusch, M.; Bello, U.D.; Carlier, S.; Colin, O.; Fernandez, V.; Gascon, F.; Hoersch, B.; Isola, C.; Laberinti, P.; Martimort, P. Sentinel-2: Esa's optical high-resolution mission for gmes operational services. *Remote Sens. Environ.* **2012**, *120*, 25–36. [CrossRef]

23. Immitzer, M.; Vuolo, F.; Atzberger, C. First experience with sentinel-2 data for crop and tree species classifications in central europe. *Remote Sens.* **2016**, *8*, 166. [CrossRef]

24. Korhonen, L.; Hadi; Packalen, P.; Rautiainen, M. Comparison of sentinel-2 and landsat 8 in the estimation of boreal forest canopy cover and leaf area index. *Remote Sens. Environ.* **2017**, *195*, 259–274. [CrossRef]

25. Shoko, C.; Mutanga, O. Examining the strength of the newly-launched sentinel 2 msi sensor in detecting and discriminating subtle differences between c3 and c4 grass species. *ISPRS J. Photogramm. Remote Sens.* **2017**, *129*, 32–40. [CrossRef]

26. Mura, M.; Bottalico, F.; Giannetti, F.; Bertani, R.; Giannini, R.; Mancini, M.; Orlandini, S.; Travaglini, D.; Chirici, G. Exploiting the capabilities of the sentinel-2 multi spectral instrument for predicting growing stock volume in forest ecosystems. *Int. J. Appl. Earth. Obs. Geoinf.* **2018**, *66*, 126–134. [CrossRef]

27. Puliti, S.; Saarela, S.; Gobakken, T.; Stahl, G.; Naesset, E. Combining uav and sentinel-2 auxiliary data for forest growing stock volume estimation through hierarchical model-based inference. *Remote Sens. Environ.* **2018**, *204*, 485–497. [CrossRef]

28. Shapiro, A.; Trettin, C.; Küchly, H.; Alavinapanah, S.; Bandeira, S. The mangroves of the zambezi delta: Increase in extent observed via satellite from 1994 to 2013. *Remote Sens.* **2015**, *7*, 16504–16518. [CrossRef]

29. Pastor-Guzman, J.; Atkinson, P.; Dash, J.; Rioja-Nieto, R. Spatiotemporal variation in mangrove chlorophyll concentration using landsat 8. *Remote Sens.* **2015**, *7*, 14530–14558. [CrossRef]

30. Valderrama-Landeros, L.; Flores-de-Santiago, F.; Kovacs, J.M.; Flores-Verdugo, F. An assessment of commonly employed satellite-based remote sensors for mapping mangrove species in mexico using an ndvi-based classification scheme. *Environ. Monit. Assess.* **2018**, *190*, 13. [CrossRef] [PubMed]

31. Asian, A.; Rahman, A.F.; Warren, M.W.; Robeson, S.M. Mapping spatial distribution and biomass of coastal wetland vegetation in indonesian papua by combining active and passive remotely sensed data. *Remote Sens. Environ.* **2016**, *183*, 65–81.

32. Almahasheer, H. Spatial coverage of mangrove communities in the arabian gulf. *Environ. Monit. Assess.* **2018**, *190*, 10. [CrossRef] [PubMed]

33. Abd-El Monsef, H.; Smith, S.E. A new approach for estimating mangrove canopy cover using landsat 8 imagery. *Comput. Electron. Agric.* **2017**, *135*, 183–194. [CrossRef]

34. Wicaksono, P. Mangrove above-ground carbon stock mapping of multi-resolution passive remote-sensing systems. *Int. J. Remote Sens.* **2017**, *38*, 1551–1578. [CrossRef]

35. Hickey, S.M.; Callow, N.J.; Phinn, S.; Lovelock, C.E.; Duarte, C.M. Spatial complexities in aboveground carbon stocks of a semi-arid mangrove community: A remote sensing height-biomass-carbon approach. *Estuar. Coast. Shelf Sci.* **2018**, *200*, 194–201. [CrossRef]

36. Cardenas, N.Y.; Joyce, K.E.; Maier, S.W. Monitoring mangrove forests: Are we taking full advantage of technology? *Int. J. Appl. Earth. Obs. Geoinf.* **2017**, *63*, 1–14. [CrossRef]

37. Song, C.; Woodcock, C.E.; Seto, K.C.; Lenney, M.P.; Macomber, S.A. Classification and change detection using landsat tm data: When and how to correct atmospheric effects? *Remote Sens. Environ.* **2001**, *75*, 230–244. [CrossRef]

38. Sun, W.; Messinger, D. Nearest-neighbor diffusion-based pan-sharpening algorithm for spectral images. *Opt. Eng.* **2013**, *53*, 013107. [CrossRef]

39. Xin, K.; Yan, K.; Gao, C.; Li, Z. Carbon storage and its influencing factors in hainan dongzhangang mangrove wetlands. *Mar. Freshwater Res.* **2018**, *69*, 771–779. [CrossRef]

40. Kamal, M.; Phinn, S.; Johansen, K. Object-based approach for multi-scale mangrove composition mapping using multi-resolution image datasets. *Remote Sens.* **2015**, *7*, 4753–4783. [CrossRef]

41. Baatz, M.; Schape, A. Multiresolution segmentation: An optimization approach for high quality multi-scale image segmentation. In *Angewandte Geographische Information Sverarbeitung XII*; Herbert Wichmann Verlag: Karhlsruhe, Germany, 2000; pp. 12–23.

42. Duro, D.C.; Franklin, S.E.; Dubé, M.G. A comparison of pixel-based and object-based image analysis with selected machine learning algorithms for the classification of agricultural landscapes using spot-5 hrg imagery. *Remote Sens. Environ.* **2012**, *118*, 259–272. [CrossRef]

43. Ji, L.; Zhang, L.; Wylie, B. Analysis of dynamic thresholds for the normalized difference water index. *Photogramm. Eng. Remote Sens.* **2009**, *75*, 1307–1317. [CrossRef]

44. Drăguţ, L.; Csillik, O.; Eisank, C.; Tiede, D. Automated parameterisation for multi-scale image segmentation on multiple layers. *ISPRS J. Photogramm. Remote Sens.* **2014**, *88*, 119–127. [CrossRef] [PubMed]

45. Zhu, Y.; Liu, K.; Liu, L.; Wang, S.; Liu, H. Retrieval of mangrove aboveground biomass at the individual species level with worldview-2 images. *Remote Sens.* **2015**, *7*, 12192–12214. [CrossRef]

46. Wicaksono, P.; Danoedoro, P.; Hartono; Nehren, U. Mangrove biomass carbon stock mapping of the karimunjawa islands using multispectral remote sensing. *Int. J. Remote Sens.* **2016**, *37*, 26–52. [CrossRef]

47. Fernandez-Manso, A.; Fernandez-Manso, O.; Quintano, C. Sentinel-2a red-edge spectral indices suitability for discriminating burn severity. *Int. J. Appl. Earth. Obs. Geoinf.* **2016**, *50*, 170–175. [CrossRef]

48. Gitelson, A.A.; Gritz, Y.; Merzlyak, M.N. Relationships between leaf chlorophyll content and spectral reflectance and algorithms for non-destructive chlorophyll assessment in higher plant leaves. *J. Plant. Physiol.* **2003**, *160*, 271–282. [CrossRef] [PubMed]

49. Haralick, R.M.; Shanmugam, K.; Dinstein, I.H. Textural features for image classification. *IEEE Trans. Syst. Man. Cybern.* **1973**, *3*, 610–621. [CrossRef]

50. Belgiu, M.; Dragut, L. Random forest in remote sensing: A review of applications and future directions. *ISPRS J. Photogramm. Remote Sens.* **2016**, *114*, 24–31. [CrossRef]

51. Breiman, L. Random forests. *Mach. Learn.* **2001**, *45*, 5–32. [CrossRef]

52. Li, M.; Ma, L.; Blaschke, T.; Cheng, L.; Tiede, D. A systematic comparison of different object-based classification techniques using high spatial resolution imagery in agricultural environments. *Int. J. Appl. Earth Obs. Geoinf.* **2016**, *49*, 87–98. [CrossRef]

53. Genuer, R.; Poggi, J.M.; Tuleau-Malot, C. Variable selection using random forests. *Pattern Recognit. Lett.* **2010**, *31*, 2225–2236. [CrossRef]

54. Gregorutti, B.; Michel, B.; Saint-Pierre, P. Correlation and variable importance in random forests. *Stat. Comput.* **2017**, *27*, 659–678. [CrossRef]

55. Li, X.; Chen, W.; Cheng, X.; Wang, L. A comparison of machine learning algorithms for mapping of complex surface-mined and agricultural landscapes using ziyuan-3 stereo satellite imagery. *Remote Sens.* **2016**, *8*, 514. [CrossRef]

56. Ng, W.-T.; Rima, P.; Einzmann, K.; Immitzer, M.; Atzberger, C.; Eckert, S. Assessing the potential of sentinel-2 and pléiades data for the detection of prosopis and vachellia spp. in kenya. *Remote Sens.* **2017**, *9*, 74. [CrossRef]

57. Rodriguez-Galiano, V.F.; Ghimire, B.; Rogan, J.; Chica-Olmo, M.; Rigol-Sanchez, J.P. An assessment of the effectiveness of a random forest classifier for land-cover classification. *ISPRS J. Photogramm.* **2012**, *67*, 93–104. [CrossRef]

58. Foody, G.M. Sample size determination for image classification accuracy assessment and comparison. *Int. J. Remote Sens.* **2009**, *30*, 5273–5291. [CrossRef]

59. Kamal, M.; Phinn, S.; Johansen, K. Characterizing the spatial structure of mangrove features for optimizing image-based mangrove mapping. *Remote Sens.* **2014**, *6*, 984–1006. [CrossRef]

60. Heumann, B.W. An object-based classification of mangroves using a hybrid decision tree—support vector machine approach. *Remote Sens.* **2011**, *3*, 2440–2460. [CrossRef]

61. Shi, T.Z.; Liu, J.; Hu, Z.W.; Liu, H.Z.; Wang, J.J.; Wu, G.F. New spectral metrics for mangrove forest identification. *Remote Sens. Lett.* **2016**, *7*, 885–894. [CrossRef]

62. Wang, L.; Sousa, W.P. Distinguishing mangrove species with laboratory measurements of hyperspectral leaf reflectance. *Int. J. Remote Sens.* **2009**, *30*, 1267–1281. [CrossRef]

63. Puissant, A.; Rougier, S.; Stumpf, A. Object-oriented mapping of urban trees using random forest classifiers. *Int. J. Appl. Earth. Obs. Geoinf.* **2014**, *26*, 235–245. [CrossRef]

64. Pelletier, C.; Valero, S.; Inglada, J.; Champion, N.; Dedieu, G. Assessing the robustness of random forests to map land cover with high resolution satellite image time series over large areas. *Int. J. Remote Sens.* **2016**, *187*, 156–168. [CrossRef]

65. Colditz, R.R. An evaluation of different training sample allocation schemes for discrete and continuous land cover classification using decision tree-based algorithms. *Remote Sens.* **2015**, *7*, 9655–9681. [CrossRef]

66. Tolosi, L.; Lengauer, T. Classification with correlated features: Unreliability of feature ranking and solutions. *Bioinformatics* **2011**, *27*, 1986–1994. [CrossRef] [PubMed]